

Tea polyphenol polymer film enables broadband optical modulation for hybrid mode-locked ultrafast fiber lasers

Wei Chen(陈伟), Kang Li(李康), Cheng Gao(高成), Qingping Hu(胡庆平), Zhengfan Li(黎征帆), Yi Xiong(熊祎), and Yunzhou Sun(孙运周)

Citation: Chin. Phys. B, 2026, 35 (**2**): 024209. DOI: 10.1088/1674-1056/ae156e
http://cpb.iphy.ac.cn; http://iopscience.iop.org/cpb

What follows is a list of articles you may be interested in

TaS_2-based saturable absorbers for *Q*-switched fiber laser applications

Qinghua Wang(汪情华), Hao Sun(孙昊), Chenhao Lu(鲁晨浩), Huiran Yang(杨慧苒), and Lu Li(李璐)
Chin. Phys. B, 2025, 34 (**7**): 074209. DOI: 10.1088/1674-1056/addcd7

Giant saturation absorption of tungsten trioxide film prepared based on the seedless layer hydrothermal method

Xiaoguang Ma(马晓光), Fangzhen Hu(胡芳珍), Xi Chen(陈希), Yimeng Wang(王艺盟), Xiaojian Hao(郝晓剑), Min Gu(顾敏), and Qiming Zhang(张启明)
Chin. Phys. B, 2023, 32 (**3**): 034212. DOI: 10.1088/1674-1056/acaf2a

Generation of wide-bandwidth pulse with graphene saturable absorber based on tapered fiber

Ren-Li Zhang(张仁栗), Jun Wang(王俊), Mei-Song Liao(廖梅松), Xia Li(李夏), Pei-Wen Guan(关珮雯), Yin-Yao Liu(刘银垚), Yan Zhou(周延), Wei-Qing Gao(高伟清)
Chin. Phys. B, 2019, 28 (**3**): 034203. DOI: 10.1088/1674-1056/28/3/034203

Mode-locked fiber laser with $MoSe_2$ saturable absorber based on evanescent field

Ren-Li Zhang(张仁栗), Jun Wang(王俊), Xiao-Yan Zhang(张晓艳), Jin-Tian Lin(林锦添), Xia Li(李夏), Pei-Wen Kuan(关珮雯), Yan Zhou(周延), Mei-Song Liao(廖梅松), Wei-Qing Gao(高伟清)
Chin. Phys. B, 2019, 28 (**1**): 014207. DOI: 10.1088/1674-1056/28/1/014207

Two-dimensional materials-decorated microfiber devices for pulse generation and shaping in fiber lasers

Zhi-Chao Luo(罗智超), Meng Liu(刘萌), Ai-Ping Luo(罗爱平), Wen-Cheng Xu(徐文成)
Chin. Phys. B, 2018, 27 (**9**): 094215. DOI: 10.1088/1674-1056/27/9/094215

Tea polyphenol polymer film enables broadband optical modulation for hybrid mode-locked ultrafast fiber lasers

Wei Chen(陈伟)[1], Kang Li(李康)[1], Cheng Gao(高成)[1], Qingping Hu(胡庆平)[1,†], Zhengfan Li(黎征帆)[2], Yi Xiong(熊祎)[1], and Yunzhou Sun(孙运周)[1,‡]

[1] *Research Group of Nonlinear Optical Science and Quantum Technology, Research Center of Nonlinear Science & Hubei Engineering Research Center for Wide Bandgap Semiconductor Materials and Devices, School of Microelectronics, Wuhan Textile University, Wuhan* 430200, *China*

[2] *School of Textile Science and Engineering, Wuhan Textile University, Wuhan* 430200, *China*

(Received 16 September 2025; revised manuscript received 9 October 2025; accepted manuscript online 21 October 2025)

Materials exhibiting broadband nonlinear optical responses are critically important for ultrafast photonics applications, particularly as saturable absorbers (SAs) that facilitate broadband optical pulse generation. In this study, tea polyphenol-polyvinyl alcohol (TP-PVA) composite films are synthesized via a polymer embedding method and employed as SAs to initiate ultrafast pulse operation in fiber lasers. The TP-PVA SA film exhibits excellent broadband saturable absorption performance at wavelengths of 1.0 μm, 1.5 μm, and 2.0 μm, with modulation depths of 54.21%, 41.41%, and 51.16%, respectively. Stable passively mode-locked pulses with pulse widths of 588 fs, 419 fs, and 743 fs are generated in Yb-, Er-, and Tm-doped fiber lasers, respectively. This work confirms the effective performance of TP-PVA as a broadband SA, and establishes a foundation for the integration of novel and sustainable materials within ultrafast photonic systems. The approach paves the way for developing compact broadband ultrafast laser systems operating in the near-infrared spectral region.

Keywords: ultrafast fiber lasers, saturable absorbers, broadband modulators, natural dyes, tea polyphenol

PACS: 42.65.–k, 42.55.Wd, 42.70.Jk, 42.60.Fc

DOI: 10.1088/1674-1056/ae156e **CSTR:** 32038.14.CPB.ae156e

1. Introduction

The rapid advancement of ultrafast photonics, characterized by the generation and manipulation of femtosecond-to-picosecond optical pulses, has significantly expanded the frontiers of scientific research and technological innovation. Within this domain, fiber lasers emerge as pivotal enabling platforms by virtue of their exceptional efficiency and operational versatility.[1–3] These characteristics have propelled their widespread adoption across diverse fields, such as telecommunications, laser micro/nano-processing, and biomedical technologies. These lasers are crucial for applications ranging from high-resolution imaging and precision material processing to forefront optical communication technologies. Fundamental to ultrafast laser systems, mode-locked fiber lasers operate via precise phase synchronization to generate ultrashort optical pulses that are critical for a wide range of advanced applications.[4,5]

Mode-locked fiber lasers leverage critical wavelength-dependent material interactions at 1.0 μm (Yb^{3+}), 1.5 μm (Er^{3+}), and 2.0 μm (Tm^{3+}), where dopant-specific transition probabilities and host matrix compatibility optimize nonlinear optical responses essential for high-efficiency pulse generation. Critical to system performance, saturable absorbers (SAs) enable mode-locking initiation and stabilization through intensity-dependent transmission. These components facilitate stable operation across both passively mode-locked and *Q*-switched regimes via the Pauli exclusion principle — wherein photon absorption saturates upon conduction band filling. Traditional real SAs, such as semiconductor saturable absorbing mirrors (SESAM),[6,7] graphene,[8] carbon nanotubes (CNTs),[9,10] topological insulators (TIs),[11–14] transition metal dichalcogenides (TMDs),[15] MXene,[16] and black phosphorus (BPs),[17] have made significant contributions. Despite their efficient modulation capabilities, the fabrication costs associated with these materials remain prohibitively high. Their synthesis typically involves intricate multi-step processes that often require specialized equipment or stringent conditions, thereby hindering widespread adoption. Moreover, these materials often face limitations in operating bandwidth, response time, stability, preparation process, and tunability. An ideal SA should provide sufficient nonlinear effects for stable laser operation with minimal losses. As the demand for more efficient and versatile modulation solutions continues to grow, there is an urgent need to explore alternative materials that can overcome these challenges.[18–22]

Leveraging intrinsic advantages including low cost, flexibility, thermal stability, solution processability, and facile film formation, organic semiconductors have been extensively

†Corresponding author. E-mail: hqp97@wtu.edu.cn

‡Corresponding author. E-mail: syz@wtu.edu.cn

© 2026 Chinese Physical Society and IOP Publishing Ltd. All rights, including for text and data mining, AI training, and similar technologies, are reserved.

implemented in photonic and electronic devices such as solar cells, organic thin-film transistors, and bistable memory systems.[23–28] Despite their pioneering role as gain media in dye lasers, conventional organic dyes suffer from fundamental limitations arising from inherent flammability, toxicity, and carcinogenic potential, which constrain their technological viability. Tea polyphenols (TPs), derived from natural sources and exhibiting environmental friendliness along with excellent optical properties, offer unique advantages for fiber laser applications.[29,30] Their chemical and thermal stability render them promising candidates for SAs, which is crucial for maintaining laser stability. However, investigations into their nonlinear optical properties remain limited, necessitating further exploration.

Polyvinyl alcohol (PVA) is characterized by high density, high crystallinity, and strong adhesion. The resulting film is flexible, smooth, oil-resistant, solvent-resistant, wear-resistant, gas-impermeable, and water-resistant after appropriate treatment. The TP-PVA SA film was prepared using a polymer embedding method,[31] and the above characteristics of PVA enable effective integration of saturable absorber materials into fiber lasers. The nonlinear optical properties of TP were characterized using a balanced synchronous twin-detector measurement system. The TP-PVA SA film enables stable mode-locking in Yb- (1030 nm/588 fs), Er- (1556 nm/419 fs), and Tm-doped (1955 nm/743 fs) fiber lasers, demonstrating broadband functionality across the 1.0–2.0 μm spectral range. Consequently, these findings advance saturable absorber design principles and open new pathways for developing sustainable ultrafast photonic systems with enhanced optical modulation capabilities.

2. Preparation and characterization of TP-PVA film

Figure 1 shows the preparation process of the TP-PVA film. 10 mg of TP compound powder was added to 5 mL of deionized water (DI) and sonicated for 1 hour using an ultrasonic cleaner. Subsequently, 0.1 g of PVA powder (1788, 100 mesh) was dissolved in 5 mL of DI. Dissolution was achieved by magnetic stirring in a water bath maintained at 96.0 °C and 1200 rpm for 1 hour. The TP solution was combined with the PVA solution, followed by sonication for 1 hour to ensure complete mixing. The resulting mixture was transferred to a cuvette and placed in a constant-temperature drying oven at 50.0 °C for 4–5 days. Following complete evaporation of the aqueous component, the residue constituted a TP-PVA composite film. This process yielded a relatively intact saturable absorption film. The film was subsequently cut to match the diameter of the fiber jumper ferrule and transferred onto the end face of the ferrule using anhydrous ethanol. The saturable absorber device was then integrated into the optical path via transmission coupling to achieve laser modulation.

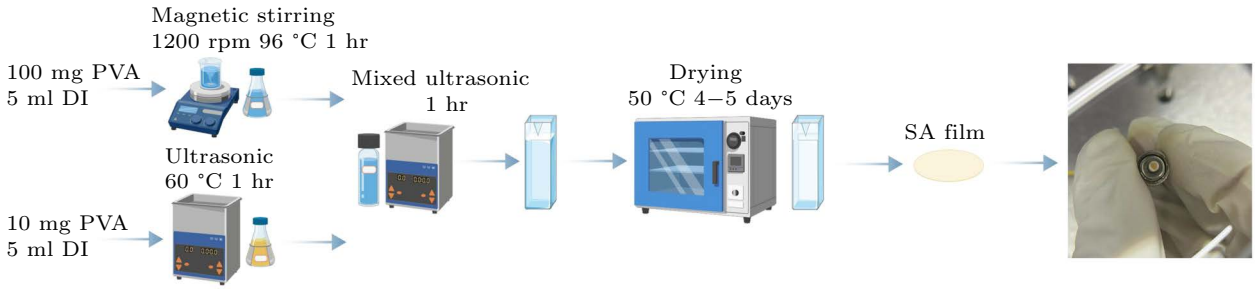


Fig. 1. Preparation process of the TP-PVA film.

The microstructure of the TP-PVA SA film was characterized using scanning electron microscopy (SEM). Figure 2(a) presents SEM images at a 10 μm scale, revealing a smooth surface devoid of significant undulations or particles, indicative of a uniform deposition process during fabrication. Figure 2(b) shows the cross-sectional energy-dispersive spectroscopy (EDS) pattern of TP, which records the content of each element. To verify the effectiveness of the TP-PVA SA, its absorption spectrum was measured using a UV-visible near-infrared spectrometer. The TP-PVA SA exhibited broadband linear absorption in the range from 900 nm to 2100 nm, as shown in Fig. 2(c). This broadband absorption contributes to the realization of ultrashort pulse generation.[32] Figure 2(d) displays the full x-ray photoelectron spectroscopy (XPS) spectrum, indicating that the sample is exclusively composed of carbon (C) and oxygen (O). The material exhibits a distinct second harmonic generation signal, demonstrating its nonlinear optical activity. High-resolution XPS spectra of C 1s and O 1s are shown in Figs. 2(e) and 2(f), respectively. The C 1s spectrum is deconvoluted into four peaks: C–C (284.8 eV), C–O (286.5 eV), C=O (289.2 eV), and a C satellite peak (292.0 eV). The O 1s spectrum reveals two peaks corresponding to C=O (532.4 eV) and C–O (533.4 eV), consistent with the C 1s fitting results. Further analysis indicates that the relative content of C=O and C–O bonds positively correlates with the nonlinear optical properties of the material.

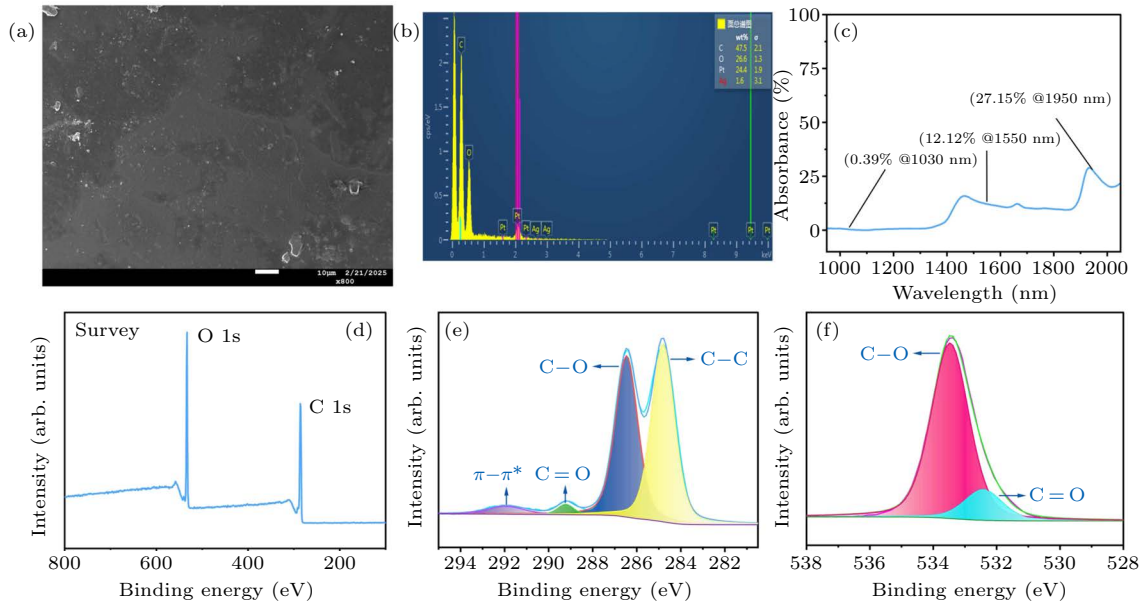


Fig. 2. Characterization of the TP-PVA SA film. (a) SEM images. (b) EDS mapping of C and O. (c) Linear absorption spectrum. (d) Full XPS survey spectrum. Fitted XPS core-level spectra of (e) C 1s and (f) O 1s.

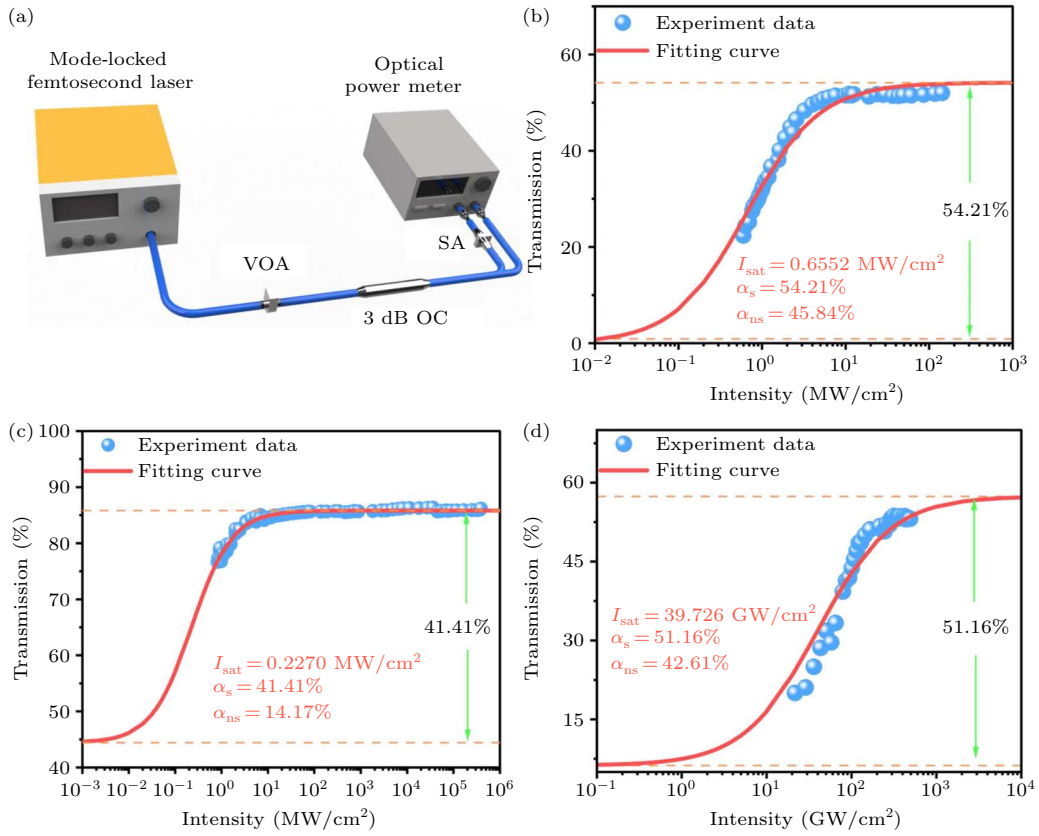


Fig. 3. Nonlinear optical characteristics of the TP-PVA SA film. (a) Schematic diagram of the balanced twin-detector device. Nonlinear optical characterization at (b) 1030 nm, (c) 1556 nm, and (d) 1955 nm.

The nonlinear optical characteristics of the TP-PVA SA at wavelengths of 1.0 μm, 1.5 μm, and 2.0 μm were studied using a balanced synchronous twin-detector measurement system, as shown in Fig. 3. At 2.0 μm, the high pulse energy and the limited accuracy of the photodetector introduce significant uncertainty in quantifying the nonlinear response of low-power signals. Although this does not affect the main conclusions regarding SA performance, more detailed investigations are planned for future work using high-sensitivity, calibrated measurement systems to further refine these quantitative results. The experimental setup is shown in Fig. 3(a). The beam emitted by a pulsed laser source is transmitted through a vari-

able optical attenuator (VOA) and introduced into an optical fiber embedded between two fiber connectors. Subsequently, a 50:50 optical coupler (OC) is connected after the attenuator to evenly split the output beam. The two output ports of the OC are connected to a fiber optic jumper incorporating the TP-PVA film and a bare fiber optic jumper without material coverage, respectively. Finally, the average optical powers at both ports are measured using optical power meters. The ratio of detected light intensities between the two outputs reflects the modulation depth of the SA.

The working wavelengths of the three laser sources used in the measurement experiment are 1030 nm, 1556 nm, and 1955 nm, respectively. The narrowest pulse widths are 560 fs, 511 fs, and 547 fs, and the repetition rates are 35.01 MHz, 25.63 MHz, and 28.21 MHz, respectively. By using a VOA to vary the input light intensity in the optical path, a series of corresponding stable average powers can be obtained. The modulation depth of the material can be determined using the following function:[14,33]

$$\alpha(I) = \frac{\alpha_s}{1 + I/I_{sat}} + \alpha_{ns}, \tag{1}$$

where $\alpha(I)$ is the absorption corresponding to the incident light intensity (I), α_s is the modulation depth, α_{ns} is the non-saturable loss, and I_{sat} is the saturation intensity. The ability of the SA to modulate pulses becomes stronger with increasing modulation depth. The fitting results are shown in Figs. 3(b)–3(d). In the 1.0 μm, 1.5 μm, and 2.0 μm bands, the saturation intensity fluences of the TP-PVA SA are 0.6552 MW/cm^2, 0.2270 MW/cm^2, and 39.726 GW/cm^2, respectively, while the modulation depths are 54.21%, 41.41%, and 51.16%, respectively. The measured non-saturable losses of the TP-PVA film are 45.84%, 14.17%, and 42.61% at 1.0 μm, 1.5 μm, and 2.0 μm, respectively. These relatively low values are beneficial for reducing the lasing threshold, as they minimize intrinsic cavity losses. The results indicate that the fabricated TP-PVA SA has the potential to be applied for mode-locking in the 1.0 μm, 1.5 μm, and 2.0 μm regions.

3. Experimental setup

In this work, to investigate the nonlinear optical properties of the TP-PVA SA, laser experimental setups based on ytterbium-doped fiber (YDF), erbium-doped fiber (EDF), and thulium-doped fiber (TDF) were established, as shown in Fig. 4. The resonant cavity lengths of the YDFL, EDFL, and TDFL experimental optical paths are 6.8 m, 8.2 m, and 7.2 m, respectively. The net group velocity dispersion (GVD) values of the YDFL, EDFL, and TDFL cavities are calculated to be 0.166 ps^2, −0.166 ps^2, and −0.180 ps^2, respectively.

A 12.5 GHz photodetector (Newport 818-BB-51F) is used to detect the output signals, which are further recorded by an 8 GHz oscilloscope (Keysight, DSOS804A). The EDFL and TDFL share the same optical spectrum analyzer (Yokogawa, AQ6375E) to monitor the spectral information, while the output signal of the YDFL is monitored by another optical spectrum analyzer (Yokogawa, AQ6370D). The average laser output power is recorded using optical power meters (Thorlabs, PM400K5). The radio-frequency (RF) spectra of the three bands are recorded using the same RF spectrum analyzer (Keysight, N9321C). A fixed non-spherical fiber collimator (LBTEK, AFC1550-2.1-APC) is used to collimate the beam for pulse width measurement, and the pulse duration is measured using autocorrelation instruments (APE pulseCheck NX50; Femtochrome, FR-103XL).

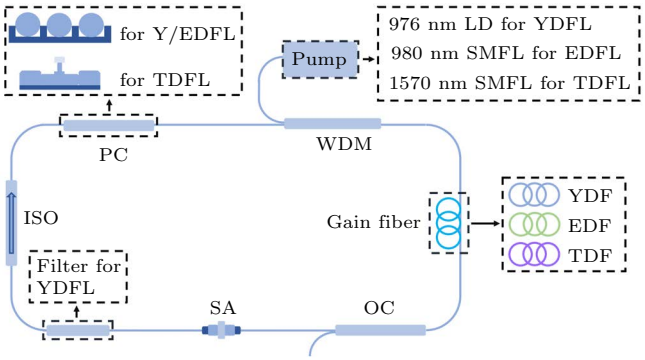


Fig. 4. Schematic diagram of Yb-, Er-, and Tm-doped mode-locked lasers. Pump: 976 nm laser for 1.0 μm, 980 nm laser for 1.5 μm, and 1570 nm laser for 2.0 μm; WDM: wavelength division multiplexer; YDF: ytterbium-doped fiber; EDF: erbium-doped fiber; TDF: thulium-doped fiber; PC: polarization controller; ISO: isolator; SA: saturable absorber; OC: output coupler; Filter: bandpass filter.

4. Broadband ultrafast photonics applications

By carefully adjusting the polarization state and pump power, all laser cavities achieved stable and continuous mode-locking operation. In Figs. 5(a)–5(c), the center wavelengths of the mode-locked pulses are located at 1029.36 nm, 1562.23 nm, and 1970.40 nm, with corresponding 3 dB spectral bandwidths of 2.77 nm, 7.20 nm, and 4.80 nm, respectively. During a continuous 12-hour spectral recording period, no significant changes were observed in the spectral profiles of the mode-locked lasers, thereby confirming the excellent long-term stability of the generated laser pulses. In the YDF laser system, the autocorrelation pulse width obtained after Gaussian fitting is 588 fs (Fig. 5(d)). In the EDF and TDF laser systems, the autocorrelation pulse widths obtained after Sech^2 fitting are 419 fs and 743 fs, respectively (Figs. 5(e) and 5(f)). Figures 6(a)–6(c) show pulse trains recorded over different time scales, including 0.5 μs for the YDF laser cavity and 1 μs for the EDF and TDF laser cavities. These long-term pulse trains clearly demonstrate the excellent stability and repeatability of the output mode-locked pulses over extended measurement periods.

In addition, shorter-scale pulse trains are presented in Figs. 6(a)–6(c), illustrating the precise temporal period of the pulses. The measured pulse periods (Figs. 6(a)–6(c)) of 32.70 ns (at 1.0 μm), 40.96 ns (at 1.5 μm), and 35.45 ns (at 2.0 μm) closely correspond to the respective cavity lengths of the fiber laser systems (Fig. 4). This remarkable consistency unambiguously demonstrates that pulse generation originates from a robust mode-locking mechanism. The radio frequency (RF) spectra of the lasers are shown in Figs. 6(d)–6(f). The stability of the mode-locked operation is further confirmed by the consistently high signal-to-noise ratio (SNR) values of 65.5 dB, 75.1 dB, and 87.0 dB for the 1.0 μm, 1.5 μm, and 2.0 μm laser cavities, respectively, as well as by the wide-range RF spectra clearly displayed in the figures.

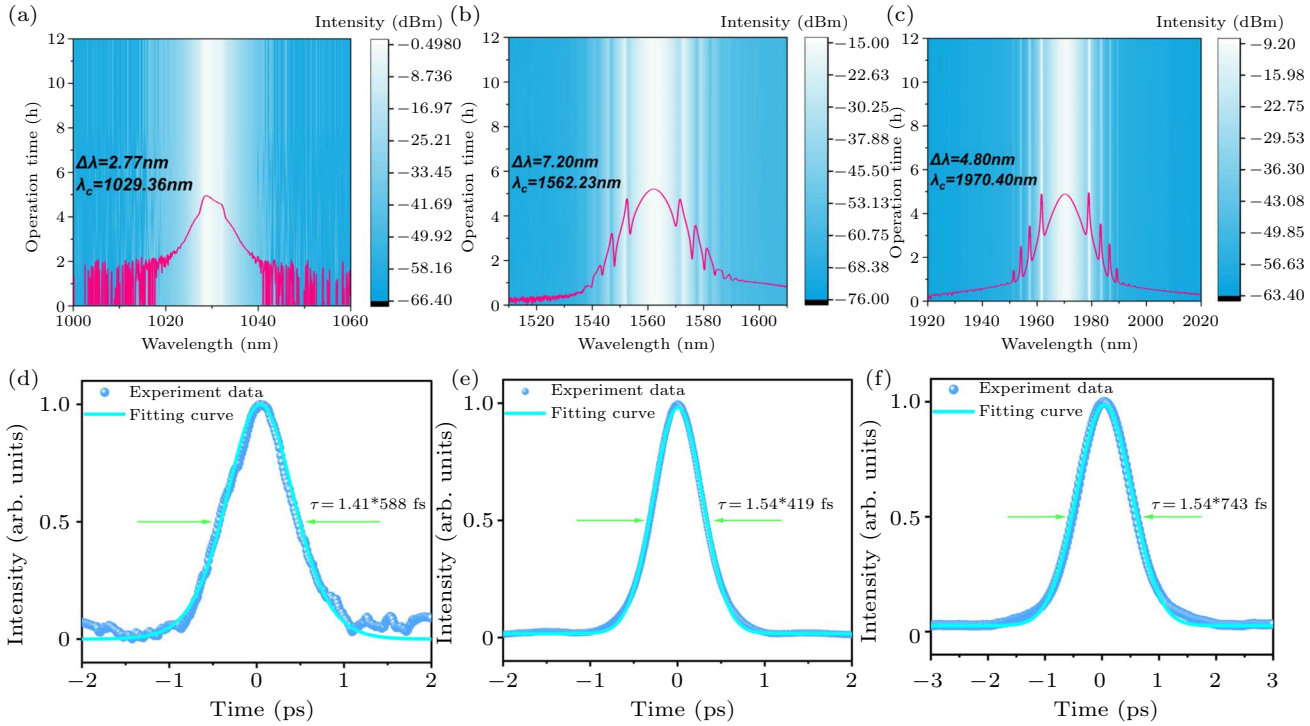


Fig. 5. Operational wavelengths of broadband mode-locked lasers with center wavelengths located at (a) 1029.36 nm (YDFL), (b) 1562.23 nm (EDFL), and (c) 1970.40 nm (TDFL). Autocorrelation traces of the output laser pulses with Gaussian fitting for (d) 1.0 μm (YDFL) and Sech^2 fitting for (e) 1.5 μm (EDFL) and (f) 2.0 μm (TDFL).

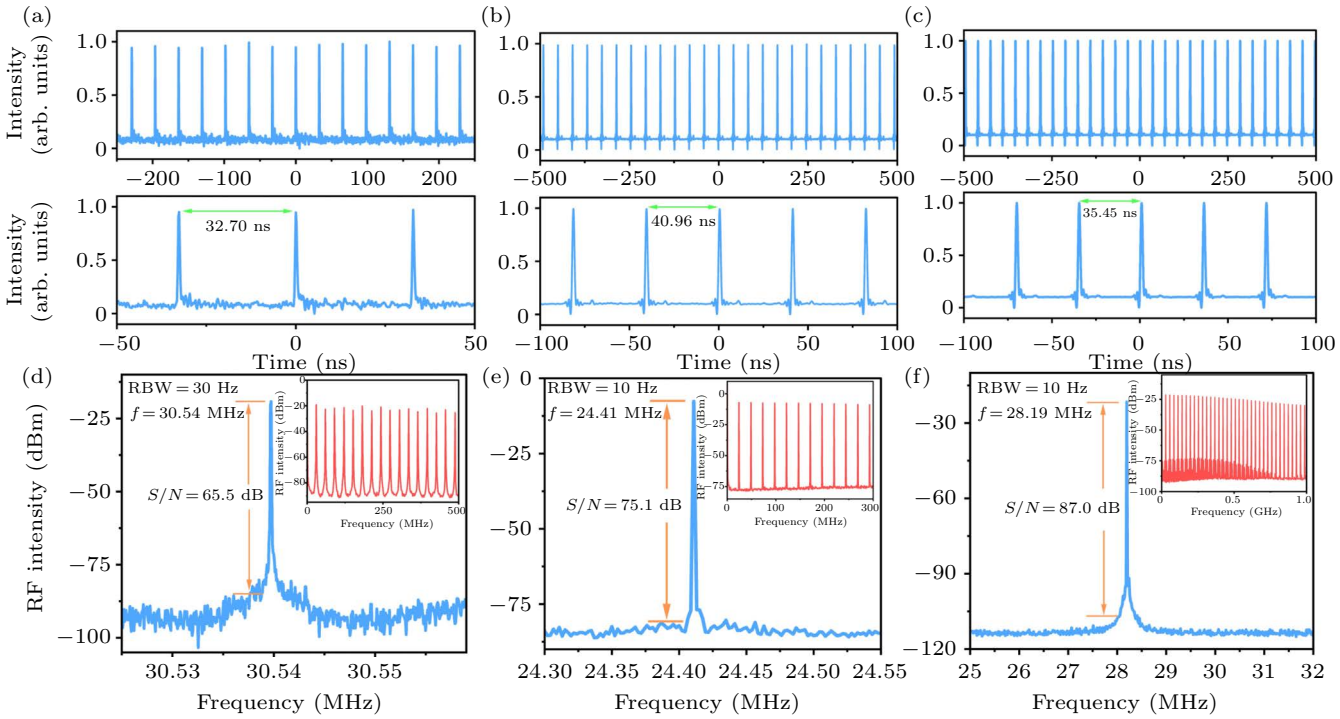


Fig. 6. Small-scale pulse trains of mode-locked lasers illustrating the pulse intervals for (a) 1.0 μm (YDFL), (b) 1.5 μm (EDFL), and (c) 2.0 μm (TDFL). RF spectra at (d) 1.0 μm (YDFL), (e) 1.5 μm (EDFL), and (f) 2.0 μm (TDFL); Inset: broad-range RF spectrum.

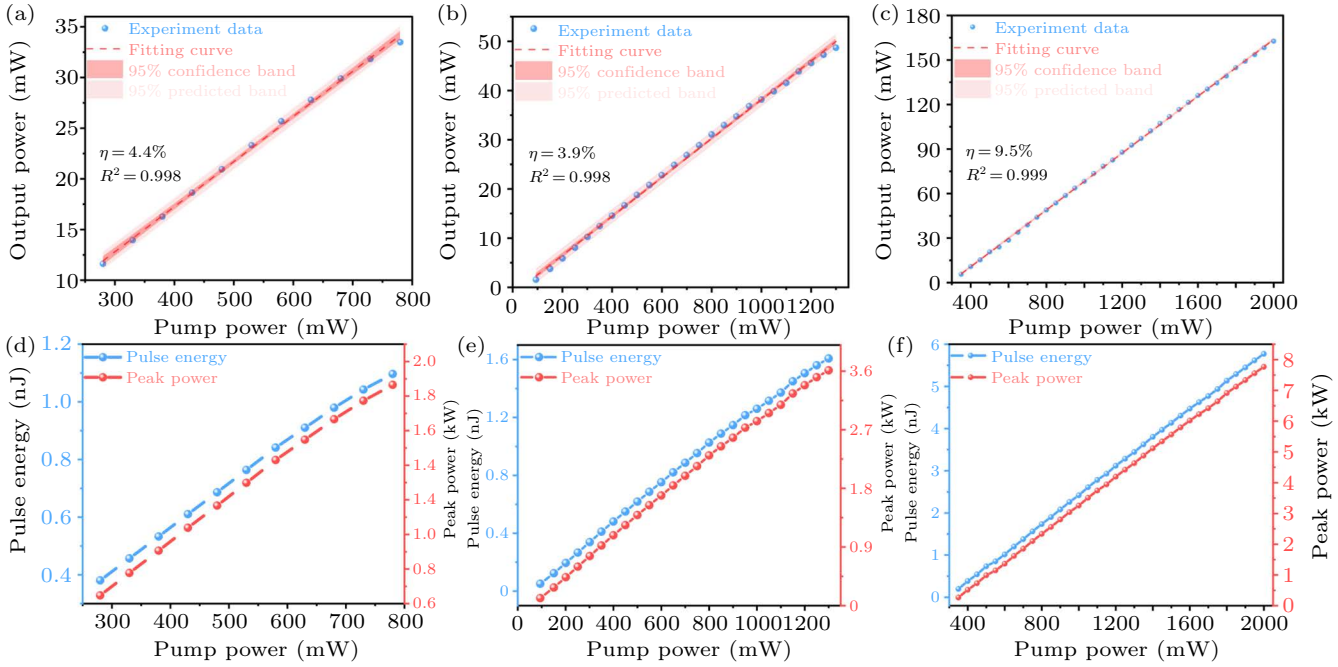


Fig. 7. Linear fitting of mode-locked laser output powers at (a) 1.0 μm (YDFL), (b) 1.5 μm (EDFL), and (c) 2.0 μm (TDFL). Single-pulse energy and peak power fitting curves for (d) 1.0 μm (YDFL), (e) 1.5 μm (EDFL), and (f) 2.0 μm (TDFL).

Table 1. Comparison of the performance of different SAs in Yb-, Er-, and Tm-doped fiber lasers.

SAs	[a]λ (μm)	[b]α_s (%)	[c]τ (fs)	[d]f_{rep} (MHz)	[e]SNR (dB)	[f]P_{output} (mW)	Refs.
GaS	1.0	10	46220	11.35	68	13.72	[32]
	1.5	5.3	614	12.35	56	4.519	
	2.0	–	1020	14.87	58.3	21.4	
Nb_2C/MoS_2	1.0	7.78	12350	18.74	65	20.5	[36]
	1.5	18.27	96.5	60.04	75	3.9	
	2.0	16.28	551	22.41	70	20	
SrFeO-NPs	1.0	19.8	801	20.37	35.46	7.31	[37]
	1.5	22	857	26.75	82	12.07	
	2.0	16.23	671	7.8	78	186.12	
TP-PVA	1.0	54.21	588	30.53	65.5	33.9	this work
	1.5	41.41	419	24.41	75.1	23.3	
	2.0	51.16	743	28.19	87	162.7	

Note: [a]λ: wavelength. [b]α_s: modulation depth. [c]τ: pulse width. [d]f_{rep}: repetition frequency. [e]SNR: signal-to-noise ratio. [f]P_{output}: output power.

The pump power thresholds of the three laser systems are 274 mW, 512 mW, and 350 mW, respectively. The highest output powers observed in the 1.0 μm, 1.5 μm, and 2.0 μm laser systems are 33.48 mW, 23.3 mW, and 162.7 mW, respectively. The corresponding conversion efficiencies (4.4%, 3.9%, and 9.5%) show a clear and nearly linear relationship between the output and pump powers, as shown in Figs. 7(a)–7(c). The peak powers are calculated as 1.86 kW (at 1.0 μm), 3.61 kW (at 1.5 μm), and 7.76 kW (at 2.0 μm), with corresponding single-pulse energies of 1.09 nJ, 0.95 nJ, and 5.77 nJ, respectively (Figs. 7(d)–7(f)). The Tm-doped fiber laser at 2.0 μm exhibits a remarkably high-power conversion efficiency of 9.5%, significantly surpassing that of the lasers at shorter wavelengths. This superior efficiency can be primarily attributed to the unique and complex energy-level dynamics of Tm^{3+} ions, particularly the efficient cross-relaxation process.[34]

The time-bandwidth product (TBP) of a soliton pulse can be theoretically calculated using the equation[35]

$$\mathrm{TBP} = \frac{\tau \times c \times \Delta\lambda}{\lambda_c^2}, \tag{2}$$

where τ is the pulse width, c is the speed of light, Δλ is the 3 dB spectral bandwidth, and λ_c is the center wavelength. The TBPs calculated from the spectral bandwidths and pulse widths are 0.461 (at 1.0 μm), 0.370 (at 1.5 μm), and 0.275 (at 2.0 μm), respectively. Deviations of the TBP from the Fourier-transform limit indicate distinct chirp dynamics and variations in pulse compression efficiency. At 1.0 μm and 1.5 μm, elevated TBPs of 0.461 and 0.370 indicate significant positive chirp accumulation due to the combined effects of the initial positive chirp from self-phase modulation (SPM) and subsequent amplification by the net normal GVD in the cavity. In contrast, the near-transform-limited TBP at 2.0 μm

(0.275) signifies efficient and highly effective pulse compression enabled by the TP-PVA SA. This sub-Fourier-limit value arises from enhanced nonlinearity that counteracts and partially reverses the dispersive chirp in the net anomalous dispersion regime. Enhanced modulation depth beyond 1.5 μm (51.16% at 2.0 μm) intensifies SPM suppression, which counteracts dispersive broadening and actively narrows the pulse duration. TBP < 0.315 (transform limit for Sech^2 pulses) occurs when nonlinear compression dominates dispersive chirp, clearly validating the superior and robust pulse-shaping capability of TP at longer wavelengths.

The distinct TBPs at 1.0 μm, 1.5 μm, and 2.0 μm arise from the strong wavelength-dependent nonlinearity of the TP-PVA SA, combined with intracavity dispersion. At 1.0 μm and 1.5 μm, under net normal dispersion, positive chirp from SPM is amplified, causing pulse broadening and higher TBPs (0.461, 0.370), while the nonlinearity of the SA is insufficient to fully counteract it. At 2.0 μm, the system operates under net anomalous dispersion, and the SA performance is substantially enhanced — its modulation depth rises to 51.16%, strengthening nonlinear compression. This enables a large nonlinear phase shift that, together with SPM, effectively compensates dispersive chirp and drives efficient soliton-like compression, yielding a near-transform-limited TBP of 0.275.

Comparison with other research results shown in Table 1 indicates that the TP-PVA SA demonstrates superior modulation depth in femtosecond mode-locked lasers, enabling shorter pulse durations than conventional saturable absorbers. Critically, the central wavelengths of the resulting fiber lasers align with the optimal absorption bands of TP, enabling highly efficient resonant absorption of the pump energy by TP ions and maximizing laser efficiency. TP possesses superior modulation depths of 54.21%, 41.41%, and 51.16%, respectively. Such high modulation depth is critical for effective optical modulation and high-quality pulse generation, surpassing the performance typically achievable with other SAs. Furthermore, the pulse widths — 588 fs (Yb), 419 fs (Er), and 743 fs (Tm) — outperform those obtained with other materials.[32,36,37] Collectively, these results confirm that TP can serve as a more efficient, stable, and robust SA material compared to currently applied materials.

5. Results and discussions

This study conclusively establishes the TP-PVA composite film as a new class of high-performance, broadband SA for ultrafast fiber lasers. Through a scalable polymer embedding method, the TP-PVA film is engineered to exhibit exceptional nonlinear optical properties across the near-infrared spectrum (1.0–2.0 μm), achieving modulation depths of 54.21% (1.0 μm), 41.41% (1.5 μm), and 51.16% (2.0 μm). The highly efficient saturable absorption characteristics of the TP-PVA SA facilitate effective control over laser pulse formation and properties, thereby enhancing overall laser performance. Crucially, the SA device enables stable, sub-750 fs mode-locked pulse generation in Yb-, Er-, and Tm-doped fiber lasers, validating its ability to unify broadband optical modulation in a sustainable material platform. The pulse-shaping capabilities of the TP-PVA SA are evidenced by near-transform-limited operation and high SNR, which directly enhance laser performance metrics, including peak power (up to 7.76 kW) and wall-plug efficiency (9.5%).

Beyond its exceptional nonlinear performance, the TP-PVA SA offers distinct practical advantages over conventional SAs,[6,38–41] in terms of material sourcing, fabrication, and environmental compatibility. Unlike SAs requiring complex epitaxial growth or chemical synthesis, TP-PVA is solution-processable and easily sourced. Its fabrication is simple, and the non-toxic, biodegradable PVA matrix offers a greener alternative to nanomaterials involving harsh chemical processing. Combining these practical benefits with broadband operation (1.0–2.0 μm) and high modulation depth, TP-PVA SA stands as a promising candidate for cost-effective and scalable ultrafast lasers in applications such as free-space communication, biomedical imaging, and material processing, where reliability and cost efficiency are critical.

Acknowledgments

This work was supported by the Opening Foundation of Hubei Key Laboratory for New Textile Materials and Applications Research (Grant No. FZXCL202410), the Key Project of Science and Technology Research Program of Hubei Provincial Department of Education, China (Grant No. D20231704), Wuhan Textile University (Grant No. 523058), and the Foundation of Wuhan Textile University (Grant No. K24058). The authors acknowledge the experimental support provided by the HX-L07 research group of the Institute of Physics, Chinese Academy of Sciences.

References

[1] Fu B, Sun J, Cheng Y, Ouyang H, Compagnini G, Yin P, Wei S, Li S, Li D, Scardaci V and Zhang H 2021 *Adv. Funct. Mater.* **31** 2107363
[2] Zhang Y, Wu K, Guang Z, Guo B, Qiao D, Wei Z, Yang H, Wang Q, Li K, Copner N and Li X 2024 *Laser Photonics Rev.* **18** 2300786
[3] Yan Y, Zhang H, Liu X, Peng L, Zhang Q, Yu G, Wu Q and Li H 2025 *Laser Photonics Rev.* **19** 2400624
[4] Liu W, Pang L, Han H, Liu M, Lei M, Fang S, Teng H and Wei Z 2017 *Opt. Express* **25** 2950
[5] Liu J, Yang F, Lu J, Ye S, Guo H, Nie H, Zhang J, He J, Zhang B and Ni Z 2022 *Nat. Commun.* **13** 3855
[6] Sharp R C, Spock D E, Pan N and Elliot J 1996 *Opt. Lett.* **21** 881
[7] Qin Z, Chai X, Xie G, Xu Z, Zhou Y, Wu Q, Li J, Wang Z, Weng Y, Hai T, Yuan P, Ma J, Chen J and Qian L 2022 *Opt. Lett.* **47** 890
[8] Zhang M, Kelleher E J R, Torrisi F, Sun Z, Hasan T, Popa D, Wang F, Ferrari A C, Popov S V and Taylor J R 2012 *Opt. Express* **20** 25077
[9] Solodyankin M A, Obraztsova E D, Lobach A S, Chernov A I, Tausenev A V, Konov V I and Dianov E M 2008 *Opt. Lett.* **33** 1336

[10] Arenal R and Lopez-Bezanilla A 2015 *WIREs Comput. Mol. Sci.* **5** 299
[11] Liu M, Wu H, Liu X, Wang Y, Lei M, Liu W, Guo W and Wei Z 2021 *Opto-Electron. Adv.* **4** 200029
[12] Liu W, Xiong X, Liu M, Xing X, Chen H, Ye H, Han J and Wei Z 2022 *Appl. Phys. Lett.* **120** 053108
[13] Xing X, Liu Y, Han J, Liu W and Wei Z 2023 *ACS Photonics* **10** 2264
[14] Jiang Y, Xing X, Zhu P, Wang K, Zhang Z, Liu Q, Wang Z, Liu W, Zhou J and Han J 2024 *J. Phys. Chem. Lett.* **15** 11419
[15] Li L, Pang L, Wang R, Zhang X, Hui Z, Han D, Zhao F and Liu W 2022 *Laser Photonics Rev.* **16** 2100255
[16] Lau K, Liu X and Qiu J 2022 *Laser Photonics Rev.* **16** 2100709
[17] Zhang Q, Jin X, Hu G, Zhang M, Zheng Z and Hasan T 2020 *Opt. Express* **28** 34104
[18] Guo B, Xiao Q, Wang S and Zhang H 2019 *Laser Photonics Rev.* **13** 1800327
[19] Jiang T, Yin K, Wang C, You J, Ouyang H, Miao R, Zhang C, Wei K, Li H, Chen H, Zhang R, Zheng X, Xu Z, Cheng X and Zhang H 2020 *Photonics Res.* **8** 78
[20] Khan K, Tareen A K, Aslam M, Wang R, Zhang Y, Mahmood A, Ouyang Z, Zhang H and Guo Z 2020 *J. Mater. Chem. C* **8** 387
[21] Li L, Cheng J, Zhao Q, Zhang J, Yang H, Zhang Y, Hui Z, Zhao F and Liu W 2023 *Opt. Express* **31** 16872
[22] Ren L, Si Z, Liu J, Sun H, Dai C, Sun H and Wang Y 2025 *ACS Appl. Mater. Interfaces* **17** 3785
[23] Rashmi M, Indira J, Sarojini B K, Mohan B J, Joe I H and Aswathy P 2021 *Opt. Laser Technol.* **139** 106902
[24] Zhang C, Li X, Wang Y, An M and Sun Z 2021 *J. Mater. Chem. C* **9** 11306
[25] Al-Hiti A S, Tiu Z C, Yasin M and Harun S W 2022 *Sci. Rep.* **12** 13288
[26] Zhang C, Li X, Chen E, Liu H, Shum P P and Chen X H 2022 *Opt. Laser Technol.* **151** 108016
[27] Salam S, Azooz S M, Nizamani B, Zhang P, Al-Masoodi A H H, Mukhtar Diblawe A, Yasin M and Harun S W 2023 *Infrared Phys. Technol.* **131** 104637
[28] Johnson V and Gandhiraj V 2024 *Opt. Mater.* **148** 114824
[29] Ramírez-Colón J L, Santiago-Maldonado X, Laboy-López S, Méndez Fernández P O, Torres-Díaz M, Lasalde-Ramírez J A, Díaz-Vázquez L M and Nicolau E 2022 *ACS Omega* **7** 2774
[30] Marchese E, Gallo Cantafio M E, Ambrosio F A, Torcasio R, Valentino I, Trapasso F, Viglietto G, Alcaro S, Costa G and Amodio N 2023 *Pharmaceuticals* **16** 1712
[31] Al-Hiti A S, Al-Masoodi A H H, Yasin M and Harun S W 2020 *Infrared Phys. Technol.* **111** 103548
[32] Ahmed S, Qiao J, Cheng P K, Saleque A M, Ivan M N A S, Alam T I and Tsang Y H 2021 *ACS Appl. Mater. Interfaces* **13** 61518
[33] Wu K, Chen B, Zhang X, Zhang S, Guo C, Li C, Xiao P, Wang J, Zhou L, Zou W and Chen J 2018 *Opt. Commun.* **406** 214
[34] Jackson S D and King T A 1998 *Opt. Lett.* **23** 1462
[35] Luo Z, Li Y, Zhong M, Huang Y, Wan X, Peng J and Weng J 2015 *Photonics Res.* **3** A79
[36] Wu Q, Peng L, Zhao J, Sun K, Chen S and Huang W 2025 *Mater. Today Phys.* **52** 101678
[37] Asghar M, Younes M H, Hayat Q, Noor A, Alrebdi T A and Asghar H 2025 *Chaos Solitons Fractals* **196** 116395
[38] Pang L, Jiang L, Zhao M, Zhang J, Zhao Q, Li L, Wu R, Lv Y and Liu W 2025 *J. Mater. Sci. Technol.* **223** 208
[39] Li L, Xue Z, Pang L, Xiao X, Yang H, Zhang J, Zhang Y, Zhao Q and Liu W 2024 *Opt. Lett.* **49** 1293
[40] Chen Y, Wu Z, Xiao P, Xiao W and Liu W 2024 *Opt. Lett.* **49** 2437
[41] Meng X C, Li L, Sun N Z, Xue Z, Liu Q, Ye H and Liu W J 2023 *Chin. Phys. Lett.* **40** 124202